frontiers in Chemistry

ORIGINAL RESEARCH
published: 18 January 2022
doi: 10.3389/fchem.2021.809415

Systematic kMC Study of Doped Hole Injection Layers in Organic Electronics

*Ali Deniz Özdemir [1†], Simon Kaiser [1†], Tobias Neumann [2], Franz Symalla [2] and Wolfgang Wenzel [1]**

[1]Institute of Nanotechnology, Karlsruhe Institute of Technology (KIT), Karlsruhe, Germany, [2]Nanomatch GmbH, Karlsruhe, Germany

Organic light emitting diodes (OLED) play an important role in commercial displays and are promising candidates for energy-efficient lighting applications. Although they have been continuously developed since their discovery in 1987, some unresolved challenges remain. The performance of OLEDs is determined by a multifaceted interplay of materials and device architectures. A commonly used technique to overcome the charge injection barrier from the electrodes to the organic layers, are doped injection layers. The optimization of doped injection layers is critical for high-efficiency OLED devices, but has been driven mainly by chemical intuition and experimental experience, slowing down the progress in this field. Therefore, computer-aided methods for material and device modeling are promising tools to accelerate the device development process. In this work, we studied the effect of doped hole injection layers on the injection barrier in dependence on material and layer properties by using a parametric kinetic Monte Carlo model. We were able to quantitatively elucidate the influence of doping concentration, material properties, and layer thickness on the injection barrier and device conductivity, leading to the conclusion that our kMC model is suitable for virtual device design.

Keywords: OLED, KMC, organic semiconductor, hole injection layer, doping

OPEN ACCESS

Edited by:
Paul Winget, Schrodinger, United States

Reviewed by:
Bronson Philippa, James Cook University, Australia
Linjun Wang, University of Mons, Belgium

****Correspondence:***
Wolfgang Wenzel
wolfgang.wenzel@kit.edu

†These authors share first authorship

Specialty section:
This article was submitted to Physical Chemistry and Chemical Physics, a section of the journal Frontiers in Chemistry

Received: *05 November 2021*
Accepted: *13 December 2021*
Published: *18 January 2022*

Citation:
Özdemir AD, Kaiser S, Neumann T, Symalla F and Wenzel W (2022) Systematic kMC Study of Doped Hole Injection Layers in Organic Electronics. Front. Chem. 9:809415. doi: 10.3389/fchem.2021.809415

1 INTRODUCTION

Since their discovery in 1987 (Tang and VanSlyke, 1987) organic light emitting diodes (OLEDs) gained lots of attention in academia and industry and have been continuously developed. Modern OLEDs find application in display technology and are promising devices for efficient general lighting applications (Adachi et al., 2000; Forrest et al., 1997). Three major factors comprise the performance and usability of OLEDs: the internal quantum efficiency (IQE), the device driving voltage (Jou et al., 2015) and light outcoupling (Flämmich et al., 2011). Common strategies to improve OLED efficiency and lifetime are based on intuition and experimental trial-and-error approaches. Quantitative models of charge injection and transfer processes in OLEDs can help to systematically increase device performance and to overcome remaining issues (Lee et al., 2017; Friederich et al., 2019; Song et al., 2020). The enormous number of potential materials and device architectures turns the development of novel materials and devices into a time- and resource-intensive task. In recent years, multiscale computational methods successfully predicted charge carrier mobility in pure materials (Friederich et al., 2014; Massé et al., 2016; Kotadiya et al., 2018) and guest-host systems (Symalla et al., 2016), current voltage characteristics (Mesta et al., 2013; Kaiser et al., 2021) and photoluminescent quenching (Symalla et al., 2020b) thus gaining relevance for the organic electronics community to be used as a supporting tool in device development and optimization (Andrienko, 2018; Friederich et al., 2019). Established simulation methods to model charge transport, charge injection (extraction)

in OLEDs are drift-diffusion methods (DD) (Rossi et al., 2020; Doan et al., 2019), macroscopic equivalent-circuit techniques (Nowy et al., 2010), and microscopic methods like kinetic Monte Carlo (kMC) or master equation approaches (ME) (Zojer, 2021). Despite their high computational costs, kMC based simulation methods emerge as a quantitative tool in device modeling (van der Holst et al., 2011; Symalla et al., 2018; Symalla et al., 2019). kMC simulations are capable of treating the charge hopping processes explicitly and to take into account electrostatic interactions with the surrounding charge carriers beyond a mean-field description (Casalegno et al., 2010; van der Holst et al., 2011; Casalegno et al., 2013; Liu et al., 2017). Another important advantage of kMC methods is the treatment of molecular doping where the coulomb interaction of charges located on neighboring molecular sites play a crucial role (Fediai et al., 2019; Fediai et al., 2020).

Doping of charge injection layers is an established technique to overcome obstacles like insufficient charge balance or limited charge carrier concentration in the device due to large charge injection barriers (Zhang and Blom, 2010; Chiba et al., 2017) and high driving voltages. However, understanding of these effects remains elusive. Therefore, we studied p-doping of hole injection layers (HIL) on the kMC level, focusing on: 1) the Fermi level alignment of the doped injection layer and 2) how the p-doping influences the conductivity of the device. Our results confirm that our kMC model is able to perform device and material simulations to systematically investigate the influence of doping concentration, material selection and layer thickness on Fermi level alignment and device conductivity.

2 METHODS

We performed the simulations on systems represented by simple cubic latices (Bässler, 1993; Pasveer et al., 2005) for each organic layer with a lattice constant was $d = 1$ nm (Mesta et al., 2013). Electronic properties like the ionization potential (IP) of the host material, electron affinity (EA) of the dopants or energetic disorder were treated as parameters and could easily be replaced by data from first-principle calculations, as done in previous works (Friederich et al., 2016; Kaiser et al., 2021). Charge carrier transport, charge injection (ejection) and doping activation with the kMC package LightForge (LF) (Symalla et al., 2016). In this approach, each microscopic process inside the device is modeled as a discrete event, with a corresponding event-rate. Each lattice site i represents an organic molecule with predefined ionization potential E_i^{IP}, electron affinity E_i^{EA} and reorganization energy λ. The energetic disorder of the organic layer is denoted by σ. Charge carrier dynamics and their interactions are treated explicitly by taking into account their Coulomb interactions explicitly. The Coulomb interaction is of particular importance in modeling doping activation (Arkhipov et al., 2005).

2.1 Charge Injection

The injection of holes from the anode to molecular site i of the organic layers is considered as a discrete process modeled with the Miller-Abrahams (Miller and Abrahams, 1960) rate to account for the ability of the electrodes to dissipate continuous amounts of energy. The expression for the injection rate $\omega_i^{(\mathrm{Inj})}$ is given by:

$$\omega_i^{(\mathrm{inj})} = \frac{\pi}{2k_{\mathrm{B}}T\hbar}|J_i^{(\mathrm{inj})}|^2 \begin{cases} \exp\left(\frac{-\Delta E_i}{4k_{\mathrm{B}}T}\right), & \text{for } \Delta E_i > 0 \\ 1\ , & \text{for } \Delta E_i \le 0 \end{cases}, \quad (1)$$

where $k_{\mathrm{B}}T$ is the thermal energy, $J_i^{(\mathrm{inj})}$ is the electronic coupling of the anode with site i. The effective hole injection barrier is given by

$$\Delta E_i = E_i^{\mathrm{IP}} - W - \phi_{\mathrm{screen}} - \phi_{\mathrm{dyn}} + eFr_i\ , \quad (2)$$

with electrode work function W, the electric field strength F and r_i the distance between site i and the electrode projected onto the field direction. To take into account the Coulomb interaction between all charge carriers in the system, we consider the dynamic Coulomb contribution to the effective injection barrier:

$$\phi_{\mathrm{dyn}} = \frac{e^2}{4\pi\epsilon_0\epsilon_r}\left(\sum_j \frac{1}{r_{ij}} - \sum_k \frac{1}{r_{ik}}\right), \quad (3)$$

where r_{ij} (r_{ik}) are the distances between the site i and all positive (negative) charges inside the device. After each kMC-step, the dynamic Coulomb interaction is recomputed by performing an Ewald-summation (Ewald, 1921). To fulfill the boundary condition of a constant electrostatic potential on the electrode surface, the screening term $\phi_{\mathrm{screen}} = -e^2\,(16\pi\epsilon_0\epsilon_r r_i)^{-1}$ has to be included to the injection barrier, where r_i is the distance of site i to the surface of the electrode. The remaining term in **Eq. 2** is the energy due to the applied electric field F. The opposite process (charge carriers hop from the organic material to electrode) is modeled analogously.

2.2 Charge Transfer

We assume that charge carriers are localized on the individual sites and that the transport from site i to site j takes place as a hopping process with the Marcus rate (Marcus, 1956):

$$\omega_{ij} = \frac{2\pi}{\hbar}|J_{ij}|^2 \frac{1}{\sqrt{4\pi\lambda k_{\mathrm{B}}T}} \exp\left(-\frac{\left(\lambda + \Delta E_{ij}\right)^2}{4\lambda k_{\mathrm{B}}T}\right), \quad (4)$$

where J_{ij} is the electronic coupling between the sites, λ the reorganization energy and ΔE_{ij} contains the difference of the site ionization potentials due to the energetic disorder, the applied electric field and the dynamic electrostatic potential like in **Eq. 2**. For the electronic coupling J_{ij} we use the empiric expression:

$$J_{ij} = j_0 \exp\left(-2\frac{r_{ij}}{a_0}\right), \quad (5)$$

where j_0 is a constant, r_{ij} is the distance between site i and j and a_0 is the coupling decay length. The values for j_0 and a_0 can be found in the supplementary information.

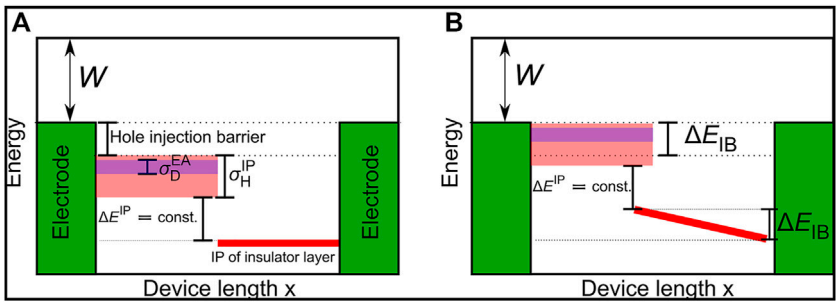

FIGURE 1 | Schematic energy level diagram of the device to measure doping induced injection barrier reduction. The device consists of two identical electrodes with the workfunction $W = 4.5$ eV and two organic layers: the doped hole injection layer (HIL) and the hole blocking layer right to it. **(A)** The host ionization potential (IP) E_H^{IP} is indicated by the light red beam with a width indicating the energetic disorder σ_H^{IP}. Analogously, the dopant electron affinity (EA) with disorder σ_D^{EA} is shown by the blue beam. **(B)** After activation of the host/dopant pairs free charge carriers (here holes) are ejected from the doped HIL into the anode, leaving a negative net charge in the organic layer and causing an upward shift of the energy levels, reducing the injection barrier. The energy levels are shifted until the tail states of the host IP reach the Fermi level of the electrodes.

2.3 Doping

The doped HIL consists of host (H) and dopant (D) sites arranged in a cubic grid with the dopant sites randomly distributed in the lattice. For p-doping, the dopant extracts an electron from a host site, leading to an ionized host and negatively charged dopant molecule:

$$H + D \rightarrow H^+ + D^- \ . \tag{6}$$

In the kMC protocol doping activation (ionization of a host/dopant pair) is treated by explicitly taking into account the Coulomb interaction V_C of the host/dopant pair and the interaction between the host/dopant pair and all other charge carriers in the device (similar to ϕ_{screen} discussed above). The doping activation energy reads:

$$\Delta E_{ion} = -\Delta E_{off} + V_C + \Delta E_{ext} \pm eFr_{HD} \ , \tag{7}$$

where the first term $\Delta E_{off} = E_D^{EA} - E_H^{IP}$ is the energy difference between dopant electron affinity E_D^{EA} and host ionization potential E_H^{IP}. The Coulomb interaction between host cation and dopant anion is given by $V_C = -e^2 (4\pi\epsilon_o\epsilon_r r_{HD})^{-1}$, where r_{HD} is the distance between the host and dopant sites. Similar to the electrostatic interactions discussed above, the ionized host/dopant pair interacts with all charge carriers inside the devices. The contribution of the explicit Coulomb interaction is given by:

$$\Delta E_{ext} = \frac{e^2}{4\pi\epsilon_0\epsilon_r}\left(\sum_\alpha\left(\frac{1}{r_{\alpha D}} - \frac{1}{r_{\alpha H}}\right) + \sum_\beta\left(\frac{1}{r_{\beta H}} - \frac{1}{r_{\beta D}}\right)\right), \tag{8}$$

where $r_{\alpha(\beta)H(D)}$ is the distance between the activated host (dopant) molecule and negative α (positive β) charge carriers inside the device. Since the dopants in the device are randomly distributed and charge carrier positions fluctuate strongly, ΔE_{ext} is a stochastic quantity and changes with each kMC step. We treat doping as charge transfer from the dopant to the host, with the doping activation rates obtained by using **Equation 4** and replacing ΔE_{ij} by ΔE_{ion}.

3 RESULTS AND DISCUSSION

3.1 Effect of Doped Injection Layer on Voltage Drop

Virtual Device for Measurement of Fermi Level Alignment

In the first part of this study we investigated the effect of the doping concentration on the hole injection barrier between the anode and the doped HIL. The schematic structure of the simulated device is shown in **Figure 1A**. It consists of two organic layers where the first one is the doped HIL and the second one serves as hole blocking layer, with a layer thickness of 15 nm each. Both electrodes have the same workfunction $W = 4.5$ eV and no external voltage is applied. After activation of the host/dopant pairs free holes are ejected into the anode, leaving a negative net charge in the organic layer, causing an upwards shift of the energy levels. This process takes place until the tail states of the organic layer align with the Fermi level of the anode. **Figure 1B** shows the energy levels of the device after Fermi level alignment. As the energy barrier between the doped injection layer and insulating layer is constant, the Fermi level alignment causes a voltage drop in the insulating layer, which is observed in a slope of the energy levels. We compute the reduction of the injection barrier ΔE_{IB} as the difference in average site energies of the first and last 1 nm–slice of the insulating layer.

Effect of Initial Injection Barrier on ΔE_{IB}

Depending on the initial injection barrier, a low doping concentration may be sufficient to reach Fermi level alignment. Therefore, we studied ΔE_{IB} in the insulating layer at different initial injection barriers and doping concentrations. This study was performed on the device displayed in **Figure 1** at

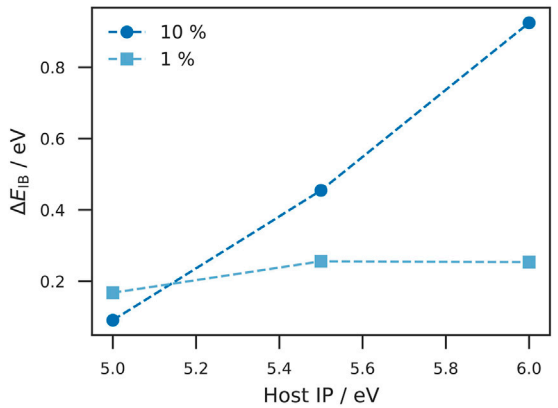

FIGURE 2 | Injection barrier reduction at different host ionization potentials and doping concentrations. The reduction of the injection barrier ΔE_{IB} is plotted against the host IP. The squares (dots) depict a doping concentration of 1% (10%). At a host IP of 5.0 eV, the observed ΔE_{IB} for 10% doping concentration is smaller than for 1% which appears unexpected. However, this can be explained by considering the fact of a doping induced increase of the energetic disorder. For small initial injection barriers, the broadening of the energy levels leads to an overlap between the tail states and the electrode Fermi level, which in turn prevents further energy alignment. Nevertheless, the difference in ΔE_{IB} is relatively small. For larger host IPs, ΔE_{IB} remains almost constant at 1% doping concentration which can be explained by the fact that not enough dopants and thus free charge carriers are available to foster Fermi level alignment. At 10% doping concentration, we observe a significant increase in ΔE_{IB} which is explained by the presence of sufficiently enough charge carriers.

different doping concentrations and energy levels of the host and dopant sites. The difference between IP and EA was kept constant at 0.5 eV to ensure equal doping efficiencies between the simulations. The simulation was performed with λ = 0.2 eV for all three site types and $\sigma^{IP}_{H(D)} = \sigma^{EA}_{H(D)}$ =0.15 eV for the host and dopant sites. The parameters for electronic couplings and the reorganization energies for charge transfer and doping activation were identical. Doping concentration has substantial impact on ΔE_{IB} as a function of host IP (see **Figure 2**). The reduction of the injecton barrier at a host IP of 5.0 eV with a doping concentration of 10% is slightly below ΔE_{IB} for 1% which can be explained by a doping induced broadening of the energy distribution in the doped injection layer (increase in energetic disorder) and the resulting overlap between the tail states and the Fermi level of the electrode. For larger initial injection barriers (larger host IP), higher doping concentration leads to a significant increase of ΔE_{IB}. While at low doping concentrations there are not enough dopants and thus free charge carriers to achieve Fermi level alignment (ΔE_{IB} at ≈0.2 eV). High doping concentrations lead to a large reduction of the injection barrier and thus good Fermi level alignment even for large initial injection barriers.

Impact of the Device Thickness on ΔE_{IB}

Besides the doping concentration, we additionally investigated the effect of the layer thickness (with constant doping concentration) on the injection barrier. **Figure 3** shows ΔE_{IB} at different doping concentrations plotted against the layer thickness. At lower doping concentrations (1–3%), we observe how the layer thickness leads to a significant increase in ΔE_{IB}. At a doping concentration of 1%, a high layer thickness leads to ΔE_{IB} from 0.1 eV to almost 0.5 eV. With increasing doping concentration, this effect becomes steadily weaker to the point where it becomes negligible: at 7 and 10% the voltage drop does not increase with the layer thickness. At a layer thickness of 15 nm, we observe a voltage drop of about 0.5 eV for all doping

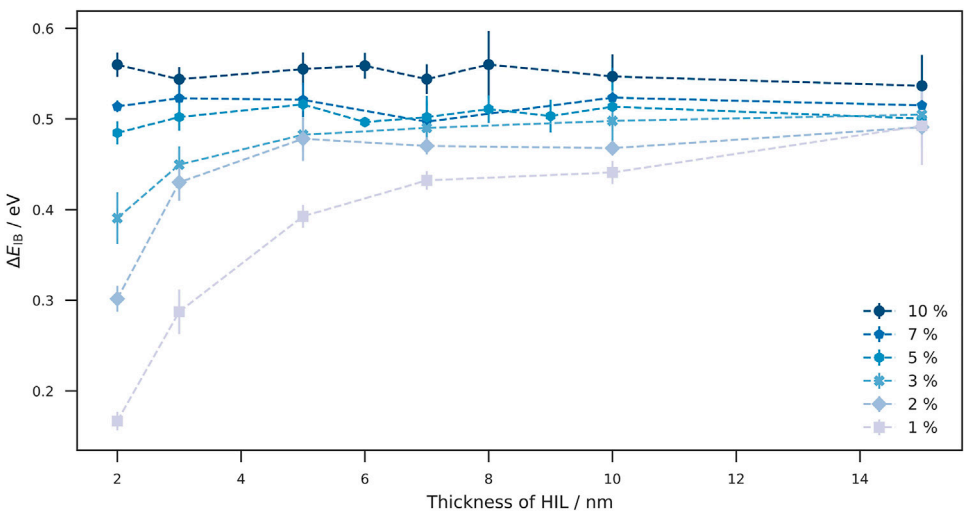

FIGURE 3 | Effect of layer thickness on the ΔE_{IB}. At a given doping concentration, the thickness of the doped injection layer controls ΔE_{IB}. While the effect of layer thickness is significant at low concentrations (1–3%), ΔE_{IB} at large doping concentration remains almost constant with increasing layer thickness. The weak variation of ΔE_{IB} at doping concentrations of 5–10% is due to the fact that sufficient dopants are already present at low layer thicknesses to provide enough charge carriers for Fermi-level alignment. A direct implication of the dependence of ΔE_{IB} on the total number of dopants is that, in addition to the doping concentration, the layer thickness of the doped injection layer can also be considered as a parameter for the reduction of the injection barrier. At maximum layer thickness, ΔE_{IB} converges to a value of about 0.5 eV, with an offset between the doping concentrations.

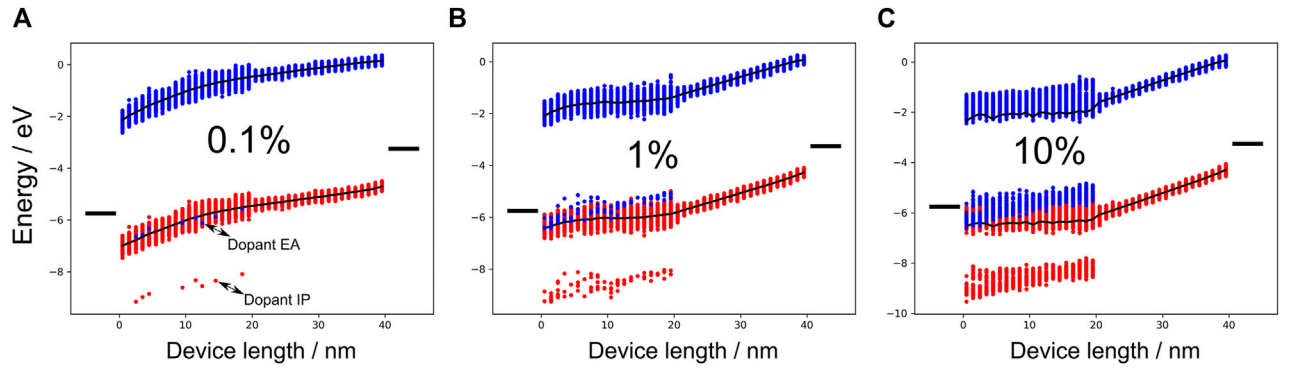

FIGURE 4 | Energy diagrams of the test device for conductivity simulations. The black bars on the left of each panel represents the Fermi level of the electrodes. The red and blue dots illustrate the IP and EA, respectively. With a doping concentration of 0.1% **(A)**, the majority of red (blue) dots represent the host IPs (EAs). The dopant IPs and EAs are explicitly annotated. At such small doping concentrations, no Fermi level alignment is achieved. With a doping concentration of 1% **(B)**, the injection barrier is significantly smaller compared to the low doping case. Fermi level alignment is accomplished at a large doping concentration of 10% **(C)**.

concentrations, with a clearly visible offset especially between the 10% curve and the others. An explanation for the offset could be the finite size effect: the site energy levels are Gaussian distributed so that the probability for host sites with tail-state energies is lower for high doping concentrations. Thus, if the tail-states are truncated, a higher energy shift is required to achieve Fermi level alignment which results in larger voltage drops in the order of the energetic disorder. These results imply, that the tendency of the doped injection layer to align with Fermi level depends on the number of intrinsically free charge carriers and thus on the number of dopants present. To increase the number of free charge carriers, there are two possibilities: increasing 1) doping concentration or 2) the layer thickness of the doped HIL.

3.2 Injection Layer Doping and Device Conductivity

Current Voltage Characteristics

In the second part of this work, we investigated how doped injection layers affect the transport properties in OLED devices. For this purpose we use a modified device with the hole blocking layer replaced by a hole transport layer (HTL) with the same energy levels as the host material in the doped HIL and a small energetic disorder of $\sigma_{\mathrm{H}}^{\mathrm{IP}}$ =0.07 eV, a common value for good hole transport materials (Aydin and Yavuz, 2021). **Figure 4** shows the energy diagram of this device with an applied electric field of 0.06 V nm^{-1} corresponding to an applied voltage of 2.4 V. With a doping concentration of 0.1% (**Figure 4A**), no Fermi level alignment is achieved which can be seen by the large injection barrier of the anode and doped HIL. As already shown in **Figures 2**, **3**, larger doping concentrations (**Figures 4B,C**) allow the reduction of the injection barrier until Fermi level alignment is reached. Another doping induced effect is where in the device the applied voltage drops. Depending on the doping concentration, most of the applied voltage drops either in the HIL or HTL. If the doping concentration is high enough, no voltage drop occurs in the injection layer, since the field is compensated for by the newly acquired free charge carriers. As a consequence, the applied voltage must drop in the neighboring insulation layer. At a doping concentration of 0.1% (see **Figure 4A**), the energy cross section in the doped HIL has a strong slope, indicating a voltage drop here. This slope is strongly reduced at 1% doping concentration and the voltage drop in the HTL increases (see **Figure 4B**). At a doping concentration of 10% the energy levels in the doped HIL are flat and the entire voltage drops in the HTL (see **Figure 4C**). Mainly, we are interested in the current density–voltage characteristics (*J–V* curve) and their dependence on the doping concentration. The current density is computed by

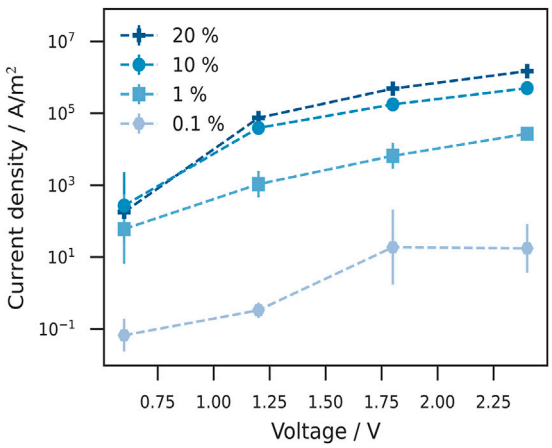

FIGURE 5 | Current voltage characteristics (*J–V*-curve) at different doping concentrations. The current density is plotted against the applied voltage. At a low doping concentration 0.1% the current density is significantly smaller than for 1% doping concentration. Higher doping concentrations (10%) lead to an further increase of the current density. The difference between the 10 and 20% JV-curves is relatively small, suggesting saturation of the doping effect on the conductivity. The results here are in line with the energy diagrams in **Figure 4**.

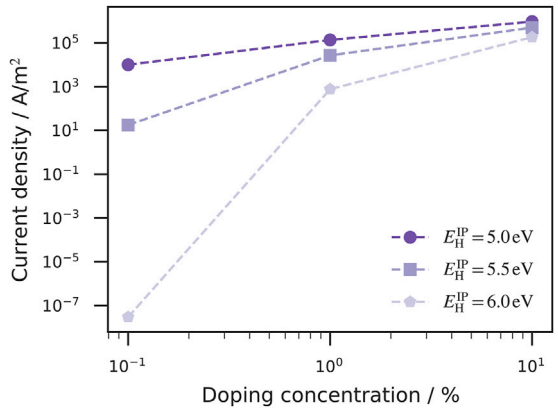

FIGURE 6 | Current density as a function of the doping concentration and host ionization potentials (IP). The relation between the IP of the host materials and the anode workfunction determine the initial hole injection barrier. At small doping concentrations (0.1%) the current density for the host material with E_H^{IP} =6.0 eV is very small compared to the current densities of the devices with other host materials (E_H^{IP} =5.0–5.5 eV). A doping concentration of 1% increases the current density of the device with E_H^{IP} =6.0 eV by nine orders of magnitude. The current enhancing effect is much weaker for the devices with lower initial injection barriers. The host materials IP plays a minor role for a large doping concentration (10%) due to achieved Fermi level alignment even for the E_H^{IP} =6.0 eV host material.

multiplying the average drift velocity of the charge carriers and dividing it through the device cross section. **Figure 5** shows the *J–V* curve at different doping concentrations. The current density increases by several orders of magnitude from 0.1 to 1%. With doping concentrations of 1–10% the increase in current density is less strong. For 10–20%, there is only a minor increase which indicates a saturation of the doping induced impact on the current density. In the work of Murat Mesta et al. (2013), the doped injection layers were approximated by electrodes with the appropriate work functions. For large doping concentrations, we carried out simulations where the doped injection layer was replaced by an effective anode with a work function equal to the ionization potential of the host material. The results can be seen in the **Supplementary Figure S1**. Even at very large doping concentrations of 49%, replacing the doped injection layer with an effective anode leads to an overestimation of the current density by a factor of 2–5. Going towards doping concentrations more relevant in experiment, the effective anode leads to an overestimation of the current density by a factor of 20–100 and an increasing deviation in field-dependence.

Current Dependence of the Host IP at Different Doping Concentration

We have already discussed that Fermi level alignment can also be achieved for host materials that have a large IP when the doping concentration is sufficiently high (see **Figure 2**). The impact on device conductivity has an even greater importance for practical work, which is why the relationship between the current density, ionization potential of the host material and doping concentration was investigated here. For a given electrode workfunction, the host IP determines the initial hole injection barrier, before Fermi level alignment takes place due host/dopant ionization. In **Figure 6**, the current density is plotted against the doping concentration at different host IPs. At a low doping concentration (0.1%), the current density for host materials with smaller IP (E_H^{IP} =5.0–5.5 eV) is eight to ten orders of magnitude larger than for the host with E_H^{IP} =6.0 eV. At a doping concentration of 1%, the enormous discrepancy between the current densities becomes much smaller. With a further increase of the doping concentration, the host IP no longer plays a role, since the initial injection barriers were almost completely eliminated for all three cases. It is particularly worth pointing out that for the host material with E_H^{IP} =6.0 eV (large initial injection barrier 1.5 eV), the current density could be increased by approximately 12 orders of magnitude by increasing the doping concentration from 0.1 to 10%. At these large doping concentrations, high current densities are achieved regardless of the host material used. The significant impact on the current density stems from two effects: 1) the increase of mobile charge carriers due to doping activation and 2) the resulting reduction of the hole injection barrier.

4 CONCLUSION

Doping of charge injection layers is an important step to control and improve overall OLED device performance. Computer-aided methods, such as the kMC model introduced here can accelerate the search for ideal host/dopant pairs and optimal device architecture. kMC methods struggle in modelling doped injection layers, because the computational effort scales badly with the number of carriers. Doped injection layers have a large number of carriers, leading to many fast processes due to the high conductivity in efficiently doped materials. For the simulation of realistic multi-layer OLEDs, most of the kMC steps are required for the doped injection layer, rendering explicit kMC simulations of full-stack devices numerically unfeasible. One way to overcome this problem is to treat doped injection layers as an effective electrode. However, this approximation is not suitable for accurate simulations of the current density, which we have shown in **Supplementary Figure S1**. Here we report on kMC simulations of the doped hole injection layer in a cubic, two-layer device that enable us to investigate the performance of the injection layer as a function of the doping concentration, the ionization potential of the host material, and the thickness of the layer.

One particular important aspect is the effect of doping the injection layer and the injection barrier on Fermi level alignment. Using the device shown in **Figure 1** we could vary a wide range of critical parameters, such as host IP or dopant concentration to provide insights into the interplay of materials and layer configurations. In fabricated devices, the injection barrier is determined by the selection of the host material. Even with this parameter predetermined, this simulation can help optimize the doping concentration for Fermi level alignment and charge balance in the emissive layer.

Our results show that our kMC model is conceptually well suited to study the influence of doped injection layers on the

device properties. We have shown in **Figure 2** that by increasing the doping concentration, Fermi level alignment can be achieved even with large host IPs. In addition, we observed that a large layer thickness (with constant doping concentration) fosters Fermi level alignment. The effect of doping on current density is of particular practical interest. We could demonstrate that increasing the doping concentration can cause the current density to increase by many orders of magnitude (see **Figure 5**).

The simulated systems can be extended from cubic to realistic structures (Neumann et al., 2013), but we note that this approximation is less severe than one might think, because the off-diagonal disorder is captured by the distribution of hopping matrix elements. When applied to novel materials, accurate EAs and IPs can be obtained using ab-initio calculations (Armleder et al., 2021) and the Coulomb interaction of host/dopant pairs can be computed quantum-mechanically (Symalla et al., 2020a). In combination with an ab-initio parametrization, this work can help to accelerate computational screening for ideal host/dopant materials in doped injection layers and optimization of material composition and layer arrangements. In crystalline organic semiconductors the description of charge transport as sequential hopping processes may be invalidated by delocalization effects, which can occur especially at high doping concentrations or materials with high mobilities (Troisi, 2011; Oberhofer et al., 2017). Mixed quantum-classical methods (Wang et al., 2015; Stafström, 2010) might be used to take into account these effects.

In order to make kMC simulations of realistic many-layer OLEDs feasible, it is necessary to treat the doped injections layer in a special way. Treating the doped injection layer as an effective anode is thus not a general solution to the problem of kMC models when simulating entire OLED stacks, so more sophisticated effective models of the doped injection layer may solve the simulation time issue more precisely.

DATA AVAILABILITY STATEMENT

The raw data supporting the conclusions of this article will be made available by the authors, without undue reservation.

AUTHOR CONTRIBUTIONS

AÖ and SK contributed equally to this work. SK, TN, FS, and WW conceived the idea and planned the theoretical calculations; SK, FS wrote and improved simulation software for this work; SK, AÖ carried out the simulations; and AÖ, SK prepared the manuscript with the inputs from all the co-authors and substantial revision from WW.

FUNDING

AÖ received funding by GRK 2450 "Scale bridging methods in computational nanoscience." SK received funding by the High-Performance Computing 2 program of the Baden-Württemberg Stiftung (Project MSMEE). WW acknowledges funding by the Deutsche Forschungsgemeinschaft (DFG) in the Research and Training Program "Tailored Scale Bridging Approaches to Computational Nanoscience" and under Germany's Excellence Strategy — 2082/1 — 390 761 711 (3DMM2O).

SUPPLEMENTARY MATERIAL

The Supplementary Material for this article can be found online at: https://www.frontiersin.org/articles/10.3389/fchem.2021.809415/full#supplementary-material

REFERENCES

Adachi, C., Baldo, M. A., Forrest, S. R., and Thompson, M. E. (2000). High-efficiency Organic Electrophosphorescent Devices with Tris(2-Phenylpyridine) iridium Doped into Electron-Transporting Materials. *Appl. Phys. Lett.* 77, 904–906. doi:10.1063/1.1306639

Andrienko, D. (2018). "Multiscale Concepts in Simulations of Organic Semiconductors," in *Handbook of Materials Modeling*. Editors W. Andreoni and S. Yip (Cham: Springer International Publishing), 1–12. doi:10.1007/978-3-319-42913-7_39-1

Arkhipov, V. I., Heremans, P., Emelianova, E. V., and Bässler, H. (2005). Effect of Doping on the Density-Of-States Distribution and Carrier Hopping in Disordered Organic Semiconductors. *Phys. Rev. B* 71, 045214. doi:10.1103/PhysRevB.71.045214

Armleder, J., Strunk, T., Symalla, F., Friederich, P., Enrique Olivares Peña, J., Neumann, T., et al. (2021). Computing Charging and Polarization Energies of Small Organic Molecules Embedded into Amorphous Materials with Quantum Accuracy. *J. Chem. Theor. Comput.* 17, 3727–3738. doi:10.1021/acs.jctc.1c00036

Aydin, G., and Yavuz, I. (2021). Intrinsic Static/Dynamic Energetic Disorders of Amorphous Organic Semiconductors: Microscopic Simulations and Device Study. *J. Phys. Chem. C* 125, 6862–6869. doi:10.1021/acs.jpcc.0c11219

Bässler, H. (1993). Charge Transport in Disordered Organic Photoconductors a Monte Carlo Simulation Study. *Phys. Stat. Sol. (B)* 175, 15–56. doi:10.1002/pssb.2221750102

Casalegno, M., Bernardi, A., and Raos, G. (2013). Numerical Simulation of Photocurrent Generation in Bilayer Organic Solar Cells: Comparison of Master Equation and Kinetic Monte Carlo Approaches. *J. Chem. Phys.* 139, 024706. doi:10.1063/1.4812826

Casalegno, M., Raos, G., and Po, R. (2010). Methodological Assessment of Kinetic Monte Carlo Simulations of Organic Photovoltaic Devices: The Treatment of Electrostatic Interactions. *J. Chem. Phys.* 132, 094705. doi:10.1063/1.3337909

Chiba, T., Pu, Y.-J., Ide, T., Ohisa, S., Fukuda, H., Hikichi, T., et al. (2017). Addition of Lithium 8-Quinolate into Polyethylenimine Electron-Injection Layer in OLEDs: Not Only Reducing Driving Voltage but Also Improving Device Lifetime. *ACS Appl. Mater. Inter.* 9, 18113–18119. doi:10.1021/acsami.7b02658

Doan, D.-H., Glitzky, A., and Liero, M. (2019). Analysis of a Drift-Diffusion Model for Organic Semiconductor Devices. *Z. Angew. Math. Phys.* 70, 55. doi:10.1007/s00033-019-1089-z

Ewald, P. P. (1921). Die Berechnung optischer und elektrostatischer Gitterpotentiale. *Ann. Phys.* 369, 253–287. doi:10.1002/andp.19213690304

Fediai, A., Emering, A., Symalla, F., and Wenzel, W. (2020). Disorder-driven Doping Activation in Organic Semiconductors. *Phys. Chem. Chem. Phys.* 22, 10256–10264. doi:10.1039/D0CP01333A

Fediai, A., Symalla, F., Friederich, P., and Wenzel, W. (2019). Disorder Compensation Controls Doping Efficiency in Organic Semiconductors. *Nat. Commun.* 10, 4547. doi:10.1038/s41467-019-12526-6

Flämmich, M., Frischeisen, J., Setz, D. S., Michaelis, D., Krummacher, B. C., Schmidt, T. D., et al. (2011). Oriented Phosphorescent Emitters Boost OLED Efficiency. *Org. Electronics* 12, 1663–1668. doi:10.1016/j.orgel.2011.06.011

Forrest, S. R., Burrows, P. E., Shen, Z., Gu, G., Bulovic, V., and Thompson, M. E. (1997). The Stacked OLED (SOLED): a New Type of Organic Device for Achieving High-Resolution Full-Color Displays. *Synth. Met.* 91, 9–13. doi:10.1016/S0379-6779(97)03966-0

Friederich, P., Fediai, A., Kaiser, S., Konrad, M., Jung, N., and Wenzel, W. (2019). Toward Design of Novel Materials for Organic Electronics. *Adv. Mater.* 31, 1808256. doi:10.1002/adma.201808256

Friederich, P., Meded, V., Poschlad, A., Neumann, T., Rodin, V., Stehr, V., et al. (2016). Molecular Origin of the Charge Carrier Mobility in Small Molecule Organic Semiconductors. *Adv. Funct. Mater.* 26, 5757–5763. doi:10.1002/adfm.201601807

Friederich, P., Symalla, F., Meded, V., Neumann, T., and Wenzel, W. (2014). Ab Initio Treatment of Disorder Effects in Amorphous Organic Materials: Toward Parameter Free Materials Simulation. *J. Chem. Theor. Comput.* 10, 3720–3725. doi:10.1021/ct500418f

Jou, J.-H., Kumar, S., Agrawal, A., Li, T.-H., and Sahoo, S. (2015). Approaches for Fabricating High Efficiency Organic Light Emitting Diodes. *J. Mater. Chem. C* 3, 2974–3002. doi:10.1039/C4TC02495H

Kaiser, S., Kotadiya, N. B., Rohloff, R., Fediai, A., Symalla, F., Neumann, T., et al. (2021). De Novo Simulation of Charge Transport through Organic Single-Carrier Devices. *J. Chem. Theor. Comput.* 17, 6416–6422. doi:10.1021/acs.jctc.1c00584

Kotadiya, N. B., Mondal, A., Xiong, S., Blom, P. W. M., Andrienko, D., and Wetzelaer, G. J. A. H. (2018). Rigorous Characterization and Predictive Modeling of Hole Transport in Amorphous Organic Semiconductors. *Adv. Electron. Mater.* 4, 1800366. doi:10.1002/aelm.201800366

Lee, S.-M., Kwon, J. H., Kwon, S., and Choi, K. C. (2017). A Review of Flexible OLEDs toward Highly Durable Unusual Displays. *IEEE Trans. Electron. Devices* 64, 1922–1931. Conference Name: IEEE Transactions on Electron Devices. doi:10.1109/TED.2017.2647964

Liu, F., van Eersel, H., Xu, B., Wilbers, J. G. E., de Jong, M. P., van der Wiel, W. G., et al. (2017). Effect of Coulomb Correlation on Charge Transport in Disordered Organic Semiconductors. *Phys. Rev. B* 96, 205203. doi:10.1103/PhysRevB.96.205203

Marcus, R. A. (1956). On the Theory of Oxidation-Reduction Reactions Involving Electron Transfer. I. *J. Chem. Phys.* 24, 966–978. doi:10.1063/1.1742723

Massé, A., Friederich, P., Symalla, F., Liu, F., Nitsche, R., Coehoorn, R., et al. (2016). Ab Initiocharge-Carrier Mobility Model for Amorphous Molecular Semiconductors. *Phys. Rev. B* 93, 195209. doi:10.1103/PhysRevB.93.195209

Mesta, M., Carvelli, M., de Vries, R. J., van Eersel, H., van der Holst, J. J. M., Schober, M., et al. (2013). Molecular-scale Simulation of Electroluminescence in a Multilayer white Organic Light-Emitting Diode. *Nat. Mater* 12, 652–658. doi:10.1038/nmat3622

Miller, A., and Abrahams, E. (1960). Impurity Conduction at Low Concentrations. *Phys. Rev.* 120, 745–755. doi:10.1103/PhysRev.120.745

Neumann, T., Danilov, D., Lennartz, C., and Wenzel, W. (2013). Modeling Disordered Morphologies in Organic Semiconductors. *J. Comput. Chem.* 34, 2716–2725. doi:10.1002/jcc.23445

Nowy, S., Ren, W., Elschner, A., Lövenich, W., and Brütting, W. (2010). Impedance Spectroscopy as a Probe for the Degradation of Organic Light-Emitting Diodes. *J. Appl. Phys.* 107, 054501. doi:10.1063/1.3294642

Oberhofer, H., Reuter, K., and Blumberger, J. (2017). Charge Transport in Molecular Materials: An Assessment of Computational Methods. *Chem. Rev.* 117, 10319–10357. doi:10.1021/acs.chemrev.7b00086

Pasveer, W. F., Cottaar, J., Tanase, C., Coehoorn, R., Bobbert, P. A., Blom, P. W. M., et al. (2005). Unified Description of Charge-Carrier Mobilities in Disordered Semiconducting Polymers. *Phys. Rev. Lett.* 94, 206601. doi:10.1103/PhysRevLett.94.206601

Rossi, D., Palazzo, D., Di Carlo, A., and Auf der Maur, M. (2020). Drift-Diffusion Study of the IQE Roll-Off in Blue Thermally Activated Delayed Fluorescence OLEDs. *Adv. Electron. Mater.* 6, 2000245. doi:10.1002/aelm.202000245

Song, J., Lee, H., Jeong, E. G., Choi, K. C., and Yoo, S. (2020). Organic Light-Emitting Diodes: Pushing toward the Limits and beyond. *Adv. Mater.* 32, 1907539. doi:10.1002/adma.201907539

Stafström, S. (2010). Electron Localization and the Transition from Adiabatic to Nonadiabatic Charge Transport in Organic Conductors. *Chem. Soc. Rev.* 39, 2484. doi:10.1039/b909058b

Symalla, F., Fediai, A., Armleder, J., Kaiser, S., Strunk, T., Neumann, T., et al. (2020a). 43-3: Ab-initio Simulation of Doped Injection Layers. *SID Symp. Dig. Tech. Pap.* 51, 630–633. doi:10.1002/sdtp.13946

Symalla, F., Friederich, P., Kaiser, S., Strunk, T., Neumann, T., and Wenzel, W. (2018). 26-4: Computer-Aided Optimization of Multilayer OLED Devices. *SID Symp. Dig. Tech. Pap.* 49, 340–342. doi:10.1002/sdtp.12556

Symalla, F., Friederich, P., Massé, A., Meded, V., Coehoorn, R., Bobbert, P., et al. (2016). Charge Transport by Superexchange in Molecular Host-Guest Systems. *Phys. Rev. Lett.* 117, 276803. doi:10.1103/PhysRevLett.117.276803

Symalla, F., Heidrich, S., Friederich, P., Strunk, T., Neumann, T., Minami, D., et al. (2020b). Multiscale Simulation of Photoluminescence Quenching in Phosphorescent OLED Materials. *Adv. Theor. Simul.* 3, 1900222. doi:10.1002/adts.201900222

Symalla, F., Heidrich, S., Kubillus, M., Strunk, T., Neumann, T., and Wenzel, W. (2019). 19-4: Boosting OLED Performance with Ab-initio Modeling of Roll-off and Quenching Processes. *SID Symp. Dig. Tech. Pap.* 50, 259–262. doi:10.1002/sdtp.12905

Tang, C. W., and VanSlyke, S. A. (1987). Organic Electroluminescent Diodes. *Appl. Phys. Lett.* 51, 913–915. doi:10.1063/1.98799

Troisi, A. (2011). Charge Transport in High Mobility Molecular Semiconductors: Classical Models and New Theories. *Chem. Soc. Rev.* 40, 2347–2358. doi:10.1039/C0CS00198H

van der Holst, J. J. M., van Oost, F. W. A., Coehoorn, R., and Bobbert, P. A. (2011). Monte Carlo Study of Charge Transport in Organic sandwich-type Single-Carrier Devices: Effects of Coulomb Interactions. *Phys. Rev. B* 83, 085206. doi:10.1103/PhysRevB.83.085206

Wang, L., Prezhdo, O. V., and Beljonne, D. (2015). Mixed Quantum-Classical Dynamics for Charge Transport in Organics. *Phys. Chem. Chem. Phys.* 17, 12395–12406. doi:10.1039/C5CP00485C

Zhang, Y., and Blom, P. W. M. (2010). Enhancement of the Hole Injection into Regioregular Poly(3-Hexylthiophene) by Molecular Doping. *Appl. Phys. Lett.* 97, 083303. doi:10.1063/1.3464560

Zojer, K. (2021). Simulation of Charge Carriers in Organic Electronic Devices: Methods with Their Fundamentals and Applications. *Adv. Opt. Mater.* 9, 2100219. doi:10.1002/adom.202100219

Conflict of Interest: Authors TN and FS were employed by the company Nanomatch GmbH.

The remaining authors declare that the research was conducted in the absence of any commercial or financial relationships that could be construed as a potential conflict of interest.

Publisher's Note: All claims expressed in this article are solely those of the authors and do not necessarily represent those of their affiliated organizations, or those of the publisher, the editors and the reviewers. Any product that may be evaluated in this article, or claim that may be made by its manufacturer, is not guaranteed or endorsed by the publisher.